Nonlinear transmission conditions for thin highly conductive interphases of curvilinear shape

Andreeva, Daria; Miszuris, Wiktoria

Published in:
Journal of the European Ceramic Society

DOI:
10.1016/j.jeurceramsoc.2018.01.032

Publication date:
2018

Citation for published version (APA):
Andreeva, D., & Miszuris, W. (2018). Nonlinear transmission conditions for thin highly conductive interphases of curvilinear shape. *Journal of the European Ceramic Society*, *38*(8), 3012-3019. https://doi.org/10.1016/j.jeurceramsoc.2018.01.032

Nonlinear transmission conditions for thin highly conductive interphases of curvilinear shape

Daria Andreeva, Wiktoria Miszuris
Department of Mathematics, Aberystwyth University
Ceredigion SY23 3BZ, Wales, UK

Abstract

We consider heat transfer problem in a composite ceramic featuring a thin nonlinear interphase layer with distinctively different characteristics (high thermal conductivity, apart from the mentioned physical size). The presence of an interphase may be problematic for the classical FEM approach in terms of technical implementation, accuracy and stability of the results. We avoid the potential issues by replacing the interphase in the model with a zero thickness imperfect nonlinear interface with two transmission conditions. These conditions are carefully derived using asymptotic analysis and aim at preserving the physical properties of the original interphase layer now absent in the model, thus ensuring an accurate solution. Numerical examples with particular attention to various physical and geometrical aspects illustrate the validity of the described approach.

1. Introduction

Composite materials are characterised by enhanced physical properties due to their structure [11, 27, 14, 15, 16, 33, 13]. These account for the widespread use composites have gained in the past decades in every possible area of application, from energy production [1, 6] to civil construction [29, 35] to electronics [41] to automotive, aeronautic and aerospace engineering [37, 40]. Many of these areas of technology are particularly conscious of safety-related issues, which makes accuracy a primary target while creating models of the composites in use. Unfortunately, the straightforward use of the classical finite element approach to modelling materials with small structural features, such as thin layers called *interphases*, often leads to undesired results, such as unrealistic and inaccurate solutions or numerical instability

[32, 26, 30, 31, 28]. This explains the need to introduce alternative ways to model such composites.

Depending on the priorities, there are several directions to take. For example, one may attempt to give a new formulation of the finite elements, as was done for the problem of heat transfer in a composite with a thin conductive interphase in [32]. This resulted in reducing the degrees of freedom and achieving faster construction of mesh and computation in comparison with the classical approach. Yet a limitation of this method was that it was not possible to have a detailed solution within the interphase region.

Another way is to simplify the structure, i.e. to replace the thin layer in the model with an object of zero thickness. For instance, Lebon and Rizzoni do so by means of a two-level model with a perfect contact interface at the first level and imperfect interface at the second one [20, 21, 36, 37]. More commonly, however, the interphase layer is represented in the model as an imperfect interface with a set of transmission conditions that simulate the physical behaviour of the original interphase [4, 5, 24, 22, 23, 26, 42]. Having developed this method for low-conductive curvilinear layers in [2, 3], we moved on to apply a similar approach for the situation when the interphase is, contrarily, highly conductive [39]. Such a setting is similar to considering composites with stiff interphases [10, 25]. The case of a highly conductive interphasial layer can be encountered, for example, in metal reinforced ceramics that have been the object of a variety of studies regarding their thermal conductivity, increased toughness and other physical parameters and processes as well as the methods of obtaining such materials [9, 18, 19, 34, 38].

It is worth mentioning that interfacial energy is often introduced within the models with zero-thickness interface [7, 8, 12, 17]. These works show the significant influence of the structure of the interface, and, particularly, the way it may affect wave propagation, including surface waves.

In the next section of this paper we formulate the considered problem and obtain the transmission conditions that we intend for use. Section3 in its turn provides the numerical examples to support our analytical results. The final section collects the drawn conclusions and the scope set for future work.

2. Problem formulation and the derivation of transmission conditions

We are considering heat transfer in a cylindrical composite with a thin highly conductive interphase of a shape close to a ring. To be precise, the boundaries are smooth closed curves of small curvature, while the centre line in a circle $r_0(\phi) = r_0$.

Initially we are trying to solve the heat transfer equation with conditions of perfect contact with the interphase:

$$\begin{aligned} \nabla \cdot (k\nabla T) + Q &= c\rho \frac{\partial T}{\partial t}, && (1)\\ [T]\,|_{\Gamma_\pm} &= 0, && (2)\\ [\mathbf{nq}]\,|_{\Gamma_\pm} &= 0. && (3) \end{aligned}$$

Fourier's law for defining the heat flux is $q = -k(T)\nabla T$.

After switching to polar coordinates (see 1,2), the boundary value problem is transformed into

$$\begin{aligned} \frac{1}{r}\frac{\partial}{\partial r}\left(kr\frac{\partial T}{\partial r}\right) + \frac{1}{r^2}\frac{\partial}{\partial \phi}\left(k\frac{\partial T}{\partial \phi}\right) + Q(\phi, T) &= c\rho\frac{\partial T}{\partial t}, && (4)\\ T_\pm - T(r_\pm, \phi, t) &= 0,\\ q_\pm + n_r^\pm k\frac{\partial}{\partial r}T(r_\pm, \phi, t) + n_\phi^\pm k\frac{1}{r_\pm}\frac{\partial}{\partial \phi}T(r_\pm, \phi, t) &= 0. \end{aligned}$$

For deriving the transmission conditions in this case, we follow our approach [3, 2] of rescaling the interphase by means of rescaling its width:

$$\tilde{h} = \frac{1}{\varepsilon}h, \qquad (5)$$

where $\tilde{h}$ becomes proportional to the sizes of the adjacent layers. At the same time, we rescale the heat source and the thermal conductivity of the interphase material

$$\tilde{Q}(T, r, \phi) = \varepsilon Q(T, r, \phi), \quad \tilde{k}(T, r, \phi) = \varepsilon k(T, r, \phi). \qquad (6)$$

This makes the interphase characteristics comparable in value with the other parameters.

Throughout this procedure, we introduce the new coordinate

$$\xi = \frac{r - r_0}{\varepsilon \tilde{h}(\phi)}, \tag{7}$$

and the normal vectors to the boundaries are, therefore,

$$n_\pm = [n_\xi^\pm, n_\phi^\pm] = \frac{[r_0(\phi) \pm 1/2\varepsilon\tilde{h}(\phi), \pm 1/2\varepsilon\tilde{h}'(\phi)]}{\sqrt{(r_0(\phi) \pm 1/2\varepsilon\tilde{h}(\phi))^2 + 1/4\varepsilon^2(\tilde{h}'(\phi))^2}}, \tag{8}$$

where the constant centre line, i.e. $r_0' = 0$, has been taken into account. We also redefine the temperature as a function of the new variable,

$$\tilde{T}(\xi, \phi, t) = T(r, \phi, t), \tag{9}$$

and, as follows from (7) and (9),

$$\frac{\partial T}{\partial r} = \frac{1}{\varepsilon\tilde{h}(\phi)} \frac{\partial \widetilde{T}}{\partial \xi}, \tag{10}$$

$$\frac{\partial T}{\partial \phi} = \frac{\partial \widetilde{T}}{\partial \phi} - \frac{r_0'(\phi) + \varepsilon\xi\tilde{h}'(\phi)}{\varepsilon\tilde{h}(\phi)} \frac{\partial \widetilde{T}}{\partial \xi}. \tag{11}$$

The described transformations bring (24_1) to the view

$$\frac{1}{(r_0 + \varepsilon\xi\tilde{h})^2} \frac{1}{\varepsilon} \Big(\frac{\partial}{\partial \phi} - \frac{\xi\tilde{h}'(\phi)}{\tilde{h}(\phi)} \frac{\partial}{\partial \xi} \Big) \Big(\widetilde{k} \Big(\frac{\partial \widetilde{T}}{\partial \phi} - \frac{\xi\tilde{h}'(\phi)}{\tilde{h}(\phi)} \frac{\partial \widetilde{T}}{\partial \xi} \Big) \Big) + \frac{1}{(r_0 + \varepsilon\xi\tilde{h})} \frac{1}{\varepsilon^3\tilde{h}^2} \frac{\partial}{\partial \xi} \Big(\widetilde{k}(r_0 + \varepsilon\xi\tilde{h}) \frac{\partial \widetilde{T}}{\partial \xi} \Big) + \frac{1}{\varepsilon} \widetilde{Q} = c\rho \frac{\partial \widetilde{T}}{\partial t}. \tag{12}$$

Here and henceforth, for the sake of brevity, we are omitting the arguments of the functions, bearing, however, in mind that in reality $\tilde{h}, \tilde{k}, \widetilde{Q}$ are all, generally speaking, non-constant.

While the form of the first condition (4_2) is obvious also in the new terms, the second one (4_3) transforms into

$$q_\pm + n_\xi^\pm \frac{1}{\varepsilon^2} \frac{\widetilde{k}}{\tilde{h}} \frac{\partial}{\partial \xi} \widetilde{T}\big(\pm\frac{1}{2}, \phi, t\big) + n_\phi^\pm \frac{(\pm 2)\widetilde{k}}{\varepsilon} \Big(\frac{\pm\frac{1}{2}\tilde{h}'}{\tilde{h}} \frac{\partial}{\partial \xi} - \frac{\partial}{\partial \phi} \Big) \widetilde{T}\big(\pm\frac{1}{2}, \phi, t\big) = 0. \tag{13}$$

We now look for a solution to this boundary value problem in the asymptotic form

$$\widetilde{T} = \widetilde{T}_0 + \varepsilon\widetilde{T}_1 + \varepsilon^2\widetilde{T}_2 + O(\varepsilon^3). \tag{14}$$

We shall also make use of the expansion of the normal vector

$$n_\pm = n_0 \pm \varepsilon n_1 + \varepsilon^2 n_2 + O(\varepsilon^3), \tag{15}$$

where

$$n_0 = [1;0], \quad n_1 = \Big[0; \frac{\tilde{h}'}{2r_0}\Big], \tag{16}$$

and of the coefficients

$$\frac{1}{(r_0+\varepsilon\xi\tilde{h})} = \frac{1}{r_0} - \frac{\xi\tilde{h}}{r_0^2}\varepsilon + \frac{\xi^2\tilde{h}^2}{r_0^3}\varepsilon^2 + O(\varepsilon^3), \tag{17}$$

$$\frac{1}{(r_0+\varepsilon\xi\tilde{h})^2} = \frac{1}{r_0^2} - \frac{2\xi\tilde{h}}{r_0^3}\varepsilon + O(\varepsilon^2). \tag{18}$$

Now let us substitute the asymptotic expansions into the boundary value problem. The governing equation will at this step be represented as a series of equations grouped by the powers of ε:

$$\varepsilon^{-3} \quad : \quad \frac{\partial}{\partial\xi}\big(\widetilde{k}\frac{\partial\widetilde{T}_0}{\partial\xi}\big) = 0, \tag{19}$$

$$\varepsilon^{-2} \quad : \quad \frac{1}{\tilde{h}}\frac{\partial}{\partial\xi}\big(\widetilde{k}\frac{\partial\widetilde{T}_1}{\partial\xi}\big) - \xi\frac{\partial}{\partial\xi}\big(\widetilde{k}\frac{\partial\widetilde{T}_0}{\partial\xi}\big) + \frac{\partial}{\partial\xi}\big(\xi\widetilde{k}\frac{\partial\widetilde{T}_0}{\partial\xi}\big) = 0, \tag{20}$$

$$\begin{aligned}\varepsilon^{-1} \quad : \quad & \frac{\xi^2}{r_0^2}\frac{\partial}{\partial\xi}\big(\widetilde{k}\frac{\partial\widetilde{T}_0}{\partial\xi}\big) - \frac{\xi}{r_0^2\tilde{h}}\frac{\partial}{\partial\xi}\big(\widetilde{k}\xi\tilde{h}\frac{\partial\widetilde{T}_0}{\partial\xi} + \widetilde{k}r_0\frac{\partial\widetilde{T}_1}{\partial\xi}\big) + \\ \frac{1}{r_0^2}\Big(\frac{\partial}{\partial\phi}\big(\widetilde{k}\frac{\partial\widetilde{T}_0}{\partial\phi}\big) \quad & - \quad \frac{\partial}{\partial\phi}\big(\frac{\xi\tilde{h}'}{\tilde{h}}\widetilde{k}\frac{\partial\widetilde{T}_0}{\partial\xi}\big) - \frac{\xi\tilde{h}'}{\tilde{h}}\frac{\partial}{\partial\xi}\big(\widetilde{k}\frac{\partial\widetilde{T}_0}{\partial\phi}\big) + \frac{\xi\tilde{h}'}{\tilde{h}}\frac{\partial}{\partial\xi}\big(\frac{\xi\tilde{h}'}{\tilde{h}}\widetilde{k}\frac{\partial\widetilde{T}_0}{\partial\xi}\big)\Big) + \\ \frac{1}{r_0\tilde{h}^2}\frac{\partial}{\partial\xi}\big(\widetilde{k}\xi\tilde{h}\frac{\partial\widetilde{T}_1}{\partial\xi} \quad & + \quad \widetilde{k}r_0\frac{\partial\widetilde{T}_2}{\partial\xi}\big) + \widetilde{Q} = 0.\end{aligned} \tag{21}$$

We note that upon substitution of the normal vector expansion,

$$q_\pm + \frac{1}{\varepsilon^2}\frac{\widetilde{k}}{\tilde{h}}\frac{\partial}{\partial\xi}\widetilde{T}\big(\pm\frac{1}{2},\phi,t\big) + \frac{\widetilde{k}\tilde{h}'}{r_0}\Big(\frac{\pm\frac{1}{2}\tilde{h}'}{\tilde{h}}\frac{\partial}{\partial\xi} - \frac{\partial}{\partial\phi}\Big)\widetilde{T}\big(\pm\frac{1}{2},\phi,t\big) = 0. \tag{22}$$

Therefore, we get in the leading terms the following boundary value problem

$$\frac{\partial}{\partial\xi}\Big(\widetilde{k}\frac{\partial\widetilde{T}_0}{\partial\xi}\Big)=0, \tag{23}$$
$$T_\pm-\widetilde{T}_0\big(\pm\frac{1}{2},\phi,t\big)=0,$$
$$\widetilde{k}\frac{\partial\widetilde{T}_0}{\partial\xi}\Big|_{\left(\pm\frac{1}{2},\phi,t\right)}=0.$$

It can be easily noticed from $\widetilde{k}\frac{\partial\widetilde{T}_0}{\partial\xi}=0$ and $\frac{\partial\widetilde{T}_0}{\partial\xi}\Big|_{\left(\pm\frac{1}{2},\phi,t\right)}=0$ that $\widetilde{T}_0(\xi,\phi,t)=\widetilde{T}_0(\phi,t)$, i.e. in the leading terms the temperature is constant with respect to the coordinate ξ. At the same time, (23_2) is already sufficient to be used as the first transmission condition. The further analysis we are conducting to obtain just the second transmission condition.

In terms of $\widetilde{T}_1$, the boundary value problem is identical to (23), which brings us to the analogous conclusion that $\widetilde{T}_1(\xi,\phi,t)=\widetilde{T}_1(\phi,t)$, or, again, there is no dependence on ξ.

We now consider the boundary value problem in terms of $\widetilde{T}_2$, bringing (21) and (22) to a simpler view

$$\frac{1}{r_0\tilde{h}^2}\frac{\partial}{\partial\xi}\Big(\widetilde{k}\frac{\partial\widetilde{T}_2}{\partial\xi}\Big)+\frac{1}{r_0^2}\Big(\frac{\partial}{\partial\phi}\big(\widetilde{k}\frac{\partial\widetilde{T}_0}{\partial\phi}\big)-\frac{\xi\tilde{h}'}{\tilde{h}}\frac{\partial}{\partial\xi}\big(\widetilde{k}\frac{\partial\widetilde{T}_0}{\partial\phi}\big)\Big)+\widetilde{Q}=0, \tag{24}$$
$$q_\pm+\frac{\widetilde{k}}{\tilde{h}}\frac{\partial\widetilde{T}_2}{\partial\xi}\Big|_{\left(\pm\frac{1}{2},\phi,t\right)}-\frac{\tilde{h}'}{r_0}\widetilde{k}\frac{\partial\widetilde{T}_0}{\partial\phi}\Big|_{\left(\pm\frac{1}{2},\phi,t\right)}=0. \tag{25}$$

Integrating (24_1) over $(-1/2,\xi)$ while introducing auxiliary functions

$$\overline{K}_\pm(\xi)=\int_{\pm1/2}^{\xi}\frac{\partial}{\partial\phi}\big(\widetilde{k}(\widetilde{T}_0,z)\frac{\partial\widetilde{T}_0}{\partial\phi}\big)dz,\quad \overline{Q}_\pm(\xi)=\int_{\pm1/2}^{\xi}\widetilde{Q}(\widetilde{T}_0,z)dz, \tag{26}$$

leads to

$$\frac{1}{\tilde{h}}\widetilde{k}\frac{\partial\widetilde{T}_2}{\partial\xi}-\frac{\xi\tilde{h}'}{r_0}\widetilde{k}\frac{\partial\widetilde{T}_0}{\partial\phi}-\frac{1}{\tilde{h}}\widetilde{k}\frac{\partial\widetilde{T}_2}{\partial\xi}\Big|_{\left(-\frac{1}{2},\phi,t\right)}-\frac{\tilde{h}'}{2r_0}\widetilde{k}\frac{\partial\widetilde{T}_0}{\partial\phi}\Big|_{\left(-\frac{1}{2},\phi,t\right)}=-\frac{\tilde{h}}{r_0}\overline{K}_-(\xi)-\tilde{h}r_0\overline{Q}_-(\xi). \tag{27}$$

The first condition (23_2) makes it possible to treat T_0 as known. Thus, substituting $\xi=\frac{1}{2}$ into (27), we can write the transmission conditions in the

final form

$$\widetilde{T}_+(\phi,t) = \widetilde{T}_-(\phi,t) = \widetilde{T}_0(\phi,t), \tag{28}$$

$$q_+ - q_- = \frac{\tilde{h}}{r_0}\overline{K}_-\left(\tfrac{1}{2}\right) + \tilde{h}r_0\overline{Q}_-\left(\tfrac{1}{2}\right) + \tfrac{1}{2}\frac{\tilde{h}'}{r_0}\frac{\partial\widetilde{T}_0}{\partial\phi}\Big|_{\left(-\frac{1}{2},\phi,t\right)}\left(\widetilde{k}\left(\tfrac{1}{2},\phi,t\right) + \widetilde{k}\left(-\tfrac{1}{2},\phi,t\right)\right) \tag{29}$$

In case the thermal conductivity and the heat source are functions of the temperature only ($\widetilde{k} = \widetilde{k}(T), \widetilde{Q} = \widetilde{Q}(T)$), the second transmission condition can be simplified to the following explicit form

$$q_+ - q_- = \frac{\tilde{h}}{r_0}\widetilde{k}(T_+)\frac{\partial^2\widetilde{T}_0}{\partial\phi^2}\Big|_{\left(\frac{1}{2},\phi,t\right)} + \tilde{h}r_0\widetilde{Q}(T_+) + \frac{\tilde{h}'}{r_0}\widetilde{k}(T_+)\frac{\partial\widetilde{T}_0}{\partial\phi}\Big|_{\left(\frac{1}{2},\phi,t\right)}. \tag{30}$$

3. Numerical results

3.1. Physical parameters

The geometry of all the following examples is in principle the same: the composite material is a cylinder with the centre at the origin, bounded by $\hat{r}$ on the inside and $R = 3\hat{r}$ on the outside, while the interphase is described by the curves

$$r_\pm(\phi) = r_0 \pm \frac{\overline{h}}{2}(2 + \sin n\phi). \tag{31}$$

Here, $\overline{h}$ is the average interphase width and r_0 is the centre line (constant). Parameter n accounts for the boundary curvature. Particularly, the case of $n = 0$ coincides with the circular interphase, while the values $n > 0$ of the parameter define boundaries of almost circular interphases (the greater n, the greater the curvature). The cases of $n = 1, n = 5, n = 10$ will be described as numerical examples. For the calculations, the value of the normalised inner radius $\hat{r}$ is taken to be 0.5.

The temperatures at the boundaries of the composite were assumed to be $\hat{T} = 300K$ at the inside ($\hat{r}$) and $T_0 = 295K$ at the outside (R). The thermal conductivities of all three layers were considered constant, $k = 23700W/mK$ within the interphase and $k_- = k_+ = 237W/mK$ in the surrounding media ([3, 26]. For the cases when the heat source does not directly depend on the angle ϕ, it was defined as $Q = Q_0(T + \beta)$ with $Q_0 = 100$ and $\beta = 50K$.

3.2. Circular interphase examples

3.2.1. Exact solution: constructing the benchmark example

In the first example, which we shall further on use as a benchmark, the interphase is a perfect circular ring, and in such a situation it is possible to find an explicit exact solution as to a one-dimensional problem. Here, the heat source depends only on the temperature and has no direct relation to the spatial coordinates. The result of such consideration is shown in Fig.1a-1d, which present three solutions: the exact analytic solution, the exact solution to the simplified problem, i.e. the one with the transmission conditions replacing the interphase, and the numerical solution obtained via COMSOL. The second one was obtained in two slightly different ways: using r_+, r_- or r_0 instead of both as boundary values. As one can see, the first way gave a slightly more precise approximation of the situation in the interphase region.

In Table.1 the numerical values of the errors are collected. Here, $\widetilde{T}$ is the solution to the simplified (imperfect interface) formulation of the problem, $\tilde{q}$ is the heat flux evaluated from it via Fourier's law, and T_c, q_c are the values of temperature and heat flux computed in COMSOL.

errors	$\Delta\widetilde{T}$	$\delta\widetilde{T}$	ΔT_C	δT_C	$\Delta\widetilde{q}$	$\delta\widetilde{q}$	Δq_C	δq_C
outer	0.029	$9.8 * 10^{-5}$	$1.7 * 10^{-7}$	$5.7 * 10^{-10}$	17.4	0.011	0.47	$3.1 * 10^{-4}$
inner	0.028	$9.4 * 10^{-5}$	$6.7 * 10^{-6}$	$2.3 * 10^{-8}$	9.73	0.012	0.074	$8.7 * 10^{-5}$

Table 1: Errors of the solution to the simplified formulation of the problem (with imperfect interface) and of the COMSOL solution at the outer and inner boundaries of the interphase region in the original formulation.

3.2.2. Verification of transmission conditions for the circular interphase

In order to have a benchmark for reference while considering the cases of more complicated geometries, the accuracy of the transmission conditions was also directly verified by substituting into them the values of the solution at boundaries and evaluating the error between the two sides of thus obtained equations.

Specifically, the errors of the first and the second conditions respectively are evaluated as

$$\delta_i = \frac{|LHS_i - RHS_i|}{\min(|LHS_i|, |RHS_i|)}, \quad i = 1, 2, \tag{32}$$

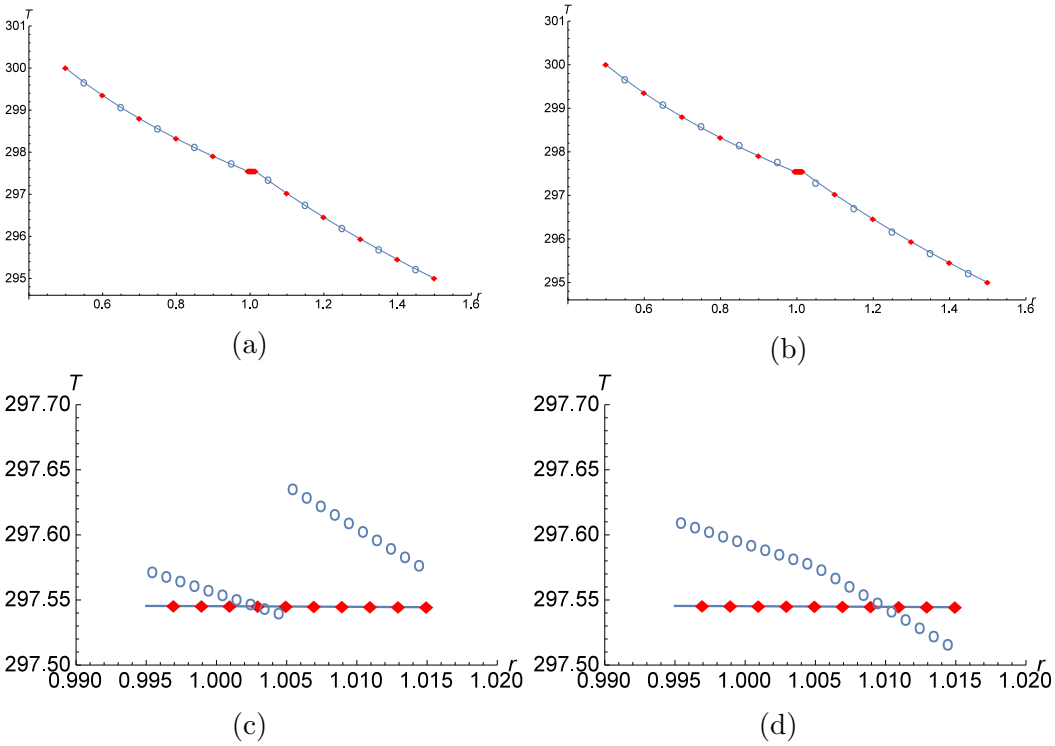

Figure 1: The exact analytical solution (solid line), COMSOL solution (diamond markers) and the solution to the simplified problem with the imperfect interface (circle markers) using r_+, r_- (a) or r_0 (b). The close-ups of the corresponding solutions in the interphase regions given in (c) and (d).

where LHS_1, RHS_1 are, naturally, just the values of the temperature solution, while

$$\begin{aligned} LHS_2 &= q_+ - q_-, \\ RHS_2 &= \frac{\tilde{h}}{r_0}\widetilde{k}(T_+)\frac{\partial^2 \widetilde{T}_0}{\partial \phi^2}\Big|_{\left(\frac{1}{2},\phi,t\right)} + \tilde{h} r_0 \widetilde{Q}(T_+) + \frac{\tilde{h}'}{r_0}\widetilde{k}(T_+)\frac{\partial \widetilde{T}_0}{\partial \phi}\Big|_{\left(\frac{1}{2},\phi,t\right)}. \end{aligned}$$

One may expect from the mere form of the transmission conditions that the first one would have a better accuracy over the second, as indeed show the numerical results collected in Table.2.

errors	ΔTC_1	δTC_1	ΔTC_2	δTC_2
exact	0.001	$3.36 * 10^{-6}$	27.06	0.04
COMSOL	0.001	$3.39 * 10^{-6}$	26.92	0.039

Table 2: Errors of the transmission conditions, verified by substituting into them the exact solution and the COMSOL numerical solution

3.2.3. Physical parameters along the boundaries of the interphase

The final step of the analysis consists of comparing the different solutions (both T and q) along the boundaries of the interphase. Naturally, the exact analytical solution and the analytical solution to the problem with the transmission conditions are both constant, since the problem is axisymmetric in both formulations and was solved as a one-dimensional one. The COMSOL solution, on the other hand, may vary along the boundaries due to the nature of the finite element structure, and thus such comparison makes perfect sense. Besides, it provides another useful method of verifying the transmission conditions which can be applied for the forthcoming cases in which obtaining the exact analytical solution proved an impossible task. We substituted the values of the COMSOL solution along a boundary into the transmission conditions, evaluated from the resulting equations the values at the other boundary and compared those to the actual values of COMSOL solution along that boundary.

Such comparison is plotted in Fig.2a-2d, where the constant solutions are represented as lines (solid blue for the original and dashed orange for the simplified formulation), while the different sets of markers stand for the COMSOL data and the values evaluated through substituting the COMSOL data into the transmission conditions.

Table3 shows the errors for temperature and heat flux for all the three: the solution to the problem with the transmission conditions, the COMSOL solution and the values obtained by substituting COMSOL data into the transmission condition. One can see that the latter have approximately the same accuracy as the transmission conditions themselves (see again Table.2). The COMSOL solution for this case has smaller errors than the solution to the problem with transmission conditions, but we should note that the latter would lead to more accurate results for yet thinner interphases, whereas the FEM model would crash at some point (as it did for this particular example

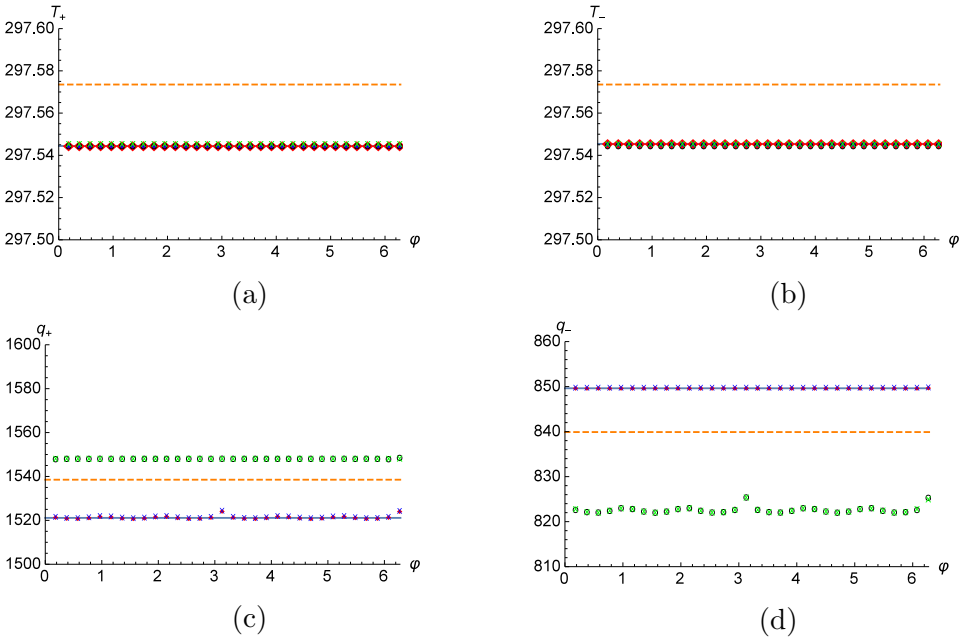

Figure 2: Temperatures (a) and (b) and heat fluxes (c) and (d) along the outer and inner boundaries for circular ($n = 0$) interphase: original formulation (solid blue line), simplified formulation with the imperfect interface conditions (dashed orange line), the COMSOL solution (diamond-shaped and X-markers), and T and q evaluated through substitution of COMSOL data into the transmission conditions (x-markers and o-markers)

for the interphase width $h = 10^{-4}$).

errors	$\delta\widetilde{T}$	δT_C	δT_{TC}	$\delta\widetilde{q}$	δq_C	δq_{TC}
outer	$9.8 * 10^{-5}$	$5.7 * 10^{-10}$	$3.4 * 10{-}6$	0.011	$3.1 * 10^{-4}$	0.018
inner	$9.4 * 10^{-5}$	$2.3 * 10^{-8}$	$3.4 * 10{-}6$	0.012	$8.7 * 10^{-5}$	0.032

Table 3: Relative errors of the values along the interphase boundaries ($\widetilde{T}, \widetilde{q}$ - exact solution to the imperfect interface formulation, T_C, q_C - COMSOL solution, T_TC, q_TC - results of the substitution of COMSOL data into the transmission conditions)

3.2.4. Case of heat source varying with the angle ϕ

We have checked whether having a heat source that depends on the angle coordinate would impair the precision of the transmission conditions. Two cases were taken into consideration: that of the heat source being dependent solely on the angle ϕ and that of the heat source described as a function of both ϕ-coordinate and temperature T. For the numerical examples described here, we took $Q(\phi) = 500(300\sin(\phi) + 300\cos(\phi) + 50)$ for the first case and $Q(\phi, T) = 500(T\sin(\phi) + T\cos(\phi) + 50)$ for the second one. Naturally, this problem can no longer be reduced to one dimension to be solved analytically, and therefore we used the previously described methods of indirect accuracy verification. Namely, we substituted the values of the COMSOL solution into the transmission conditions and evaluated the errors of between the right and left hand sides of the equations, as described in (32-33). Table.4 gives the numerical results of such comparison. The values for $Q = Q(T)$ are those from the previous example added here as a benchmark.

errors	ΔTC_1	δTC_1	ΔTC_2	δTC_2
$Q = Q(T)$	0.001	$3.39 * 10^{-6}$	26.92	0.039
$Q = Q(\phi)$	0.037	$1.2 * 10^{-4}$	218.59	0.093
$Q = Q(\phi, T)$	0.035	$1.2 * 10^{-4}$	217.72	0.1

Table 4: Errors of the transmission conditions, verified by substituting into them the COMSOL numerical solution

We note that the values of the heat source were closer between the two angle-dependent cases than to the values of heat source dependent only on temperature. Nevertheless, a clear decline in the accuracy of the transmission conditions with the introduction of the link to the spatial coordinates cannot be unnoticed. At the same time, once the heat source does depend on the coordinate ϕ, the precision of the results does not seem to be influenced by an additional dependence on the temperature.

3.3. Almost circular interphase examples

In order to investigate the effect the geometry, or, to be precise, the curvature of the interphase boundaries (which, may one bear in mind, we assumed to be small) has on the imperfect interface approach, we considered a series of examples where the centre line is still a circle while the boundaries

are only close to circular, as described by (31). Their curvature increases with the growth of the parameter n, thus allowing us to see the importance of our assumption by juxtaposing analogous numerical examples for which only the value of n varies. We therefore took the same parameter values for all the calculations as described in Subsection3.1 for the circular case. The latter corresponds to the $n = 0$ instance, which we add to the forthcoming numerical results as a benchmark. The other instances considered include $n = 1, 5, 10$ (see Fig.3).

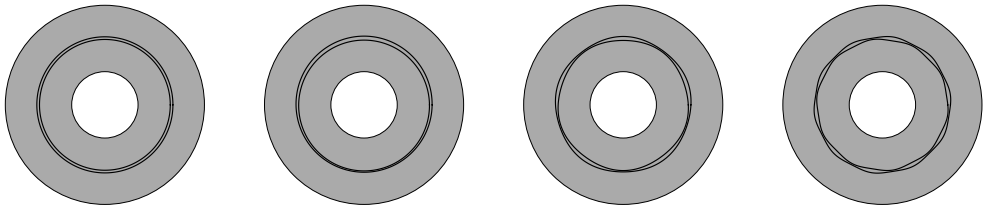

Figure 3: The domains with almost circular highly conductive interphases ($n = 0, 1, 5, 10$)

As was explained for the angle-dependent cases, these examples cannot be reduced to a one-dimensional formulation. Therefore, we could not evaluate the exact analytical solution either to the original problem or to the simplified one with the imperfect interface, and thus had to contend with the numerical solution from COMSOL, which proved to be sufficiently accurate in case $n = 0$. We then used the indirect ways of transmission conditions verification, described in Subsections3.2.2-3.2.3, to test the precision in these examples.

3.3.1. Verification of transmission conditions for the almost circular interphases

The first way of transmission conditions verification is through substituting the COMSOL solutions into the transmission conditions and calculating the errors via formulae (32-33). The first two columns of Table5, δTC_1 and δTC_2, contain the evaluated errors. It can be clearly seen how increasing the curvature of the interphase boundaries causes a fairly radical decline in the precision.

relative errors	δTC_1	δTC_2	δT_+	δT_-	δq_+	δq_-
$n = 0$	$3.4 * 10^{-6}$	0.039	$3.4 * 10^{-6}$	$3.4 * 10^{-6}$	0.018	0.032
$n = 1$	$3.4 * 10^{-6}$	0.061	$3.4 * 10^{-6}$	$3.4 * 10^{-6}$	0.027	0.051
$n = 5$	$3.4 * 10^{-6}$	0.083	$3.4 * 10^{-6}$	$3.4 * 10^{-6}$	0.035	0.066
$n = 10$	$3.4 * 10^{-6}$	0.151	$3.4 * 10^{-6}$	$3.4 * 10^{-6}$	0.06	0.11

Table 5: Precision of the transmission conditions, verified by substituting into them the COMSOL solution, as well as the precision of the data evaluated through the transmission conditions from the COMSOL solution)

3.3.2. Physical parameters along the boundaries of the interphase

Our observation is confirmed by the second way of transmission conditions verification, i.e. substitution of the COMSOL solution at one boundary into the conditions and evaluating T and q at the other boundary. The relative errors of such values in comparison with the COMSOL-calculated ones, for the lack of the exact analytical solution, are given in columns 3-6 of Table5. These once again demonstrate the increase of error with the increase of boundary curvature. For further evidence, Fig.4a-6d with the plots of the calculated values are provided.

We also noted the greater accuracy in all the considered examples of the results at the outer boundary as opposed to the inner one. Our hypothesis is that this is due to the overly refined mesh in the region, which goes in line with a similar effect of the mesh we described while dealing with an interphase with low thermal conductivity [3]. Other than this, however, the mesh did not produce a noticeable effect on the accuracy of the results.

4. Conclusions and discussion

This work was aiming at obtaining transmission conditions that could successfully replace a thin highly conductive interphase in a numerical model, which was achieved for layers of circular and almost circular shape (granted that the centre line remains a circle). The validity of such conditions was then thoroughly examined (as one has seen in the numerical examples in Section3). In particular, it can be observed that

- as we expected, the accuracy of the conditions depends on the curvature of the interphase boundary (by varying the parameter n, which

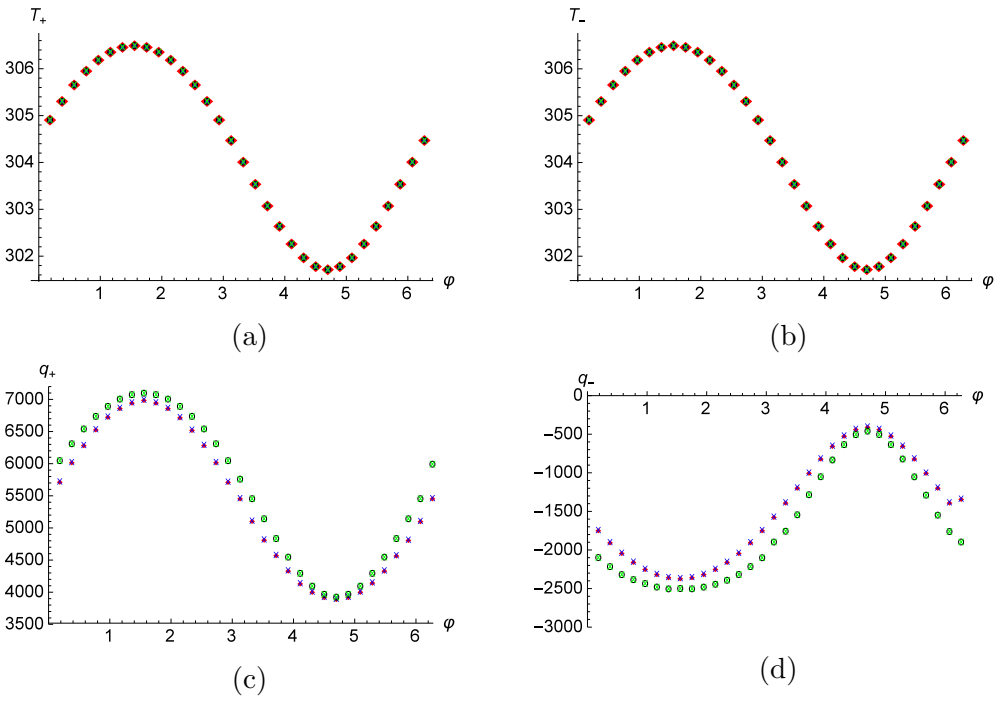

Figure 4: Temperatures (a) and (b) and heat fluxes (c) and (d) along the outer and inner boundaries for $n = 1$: the COMSOL solution (diamond-shaped and X-markers) and T and q evaluated through substitution of COMSOL data into the transmission conditions (x-markers and o-markers)

accounts for the curvature, from 0 to 10, we observed that the relative error deteriorated from 3.9% to 15.1%). This means that for layers with greater curvature further analysis would be necessary;

- the physical characteristics of the interphase also play their role in the validity of the approach. Introducing an additional dependence of the heat source on spatial coordinates, namely, the angle ϕ, led to a decline in the precision of the transmission conditions, which again calls for further analysis;

- there are two different ways to use the transmission conditions, taking either the values at the interphase boundaries or at its centre line. This has little influence on the accuracy of the solution, so one can choose whichever way, depending on the desired continuity of the solution.

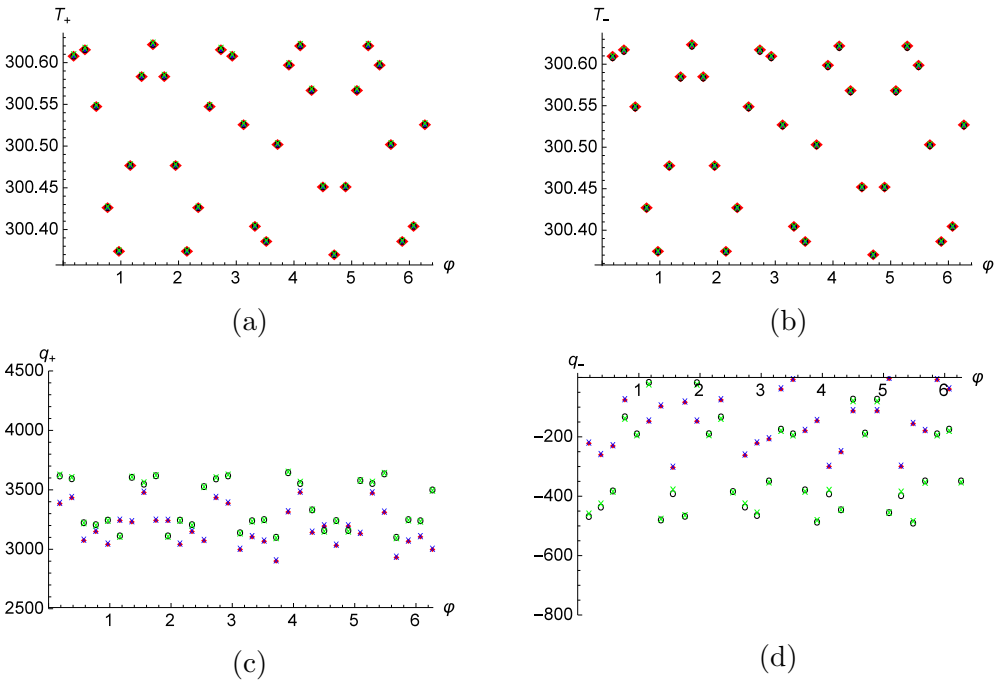

Figure 5: Temperatures (a) and (b) and heat fluxes (c) and (d) along the outer and inner boundaries for $n = 5$: the COMSOL solution (diamond-shaped and X-markers) and T and q evaluated through substitution of COMSOL data into the transmission conditions (x-markers and o-markers)

5. Acknowledgements

The authors acknowledge the FP7 Marie Curie project TAMER for the financial support of their research.

References

[1] Agnese, F., Scarpa, F., 2014. Macro-composites with star-shaped inclusions for vibration damping in wind turbine blades. Composite Structures 108, 978–986.

[2] Andreeva, D., Miszuris, W., 2017. Nonlinear transmission conditions for thin curvilinear low-conductive interphases. Continuum Mechanics and Thermodynamics 29 (1), 345–358.

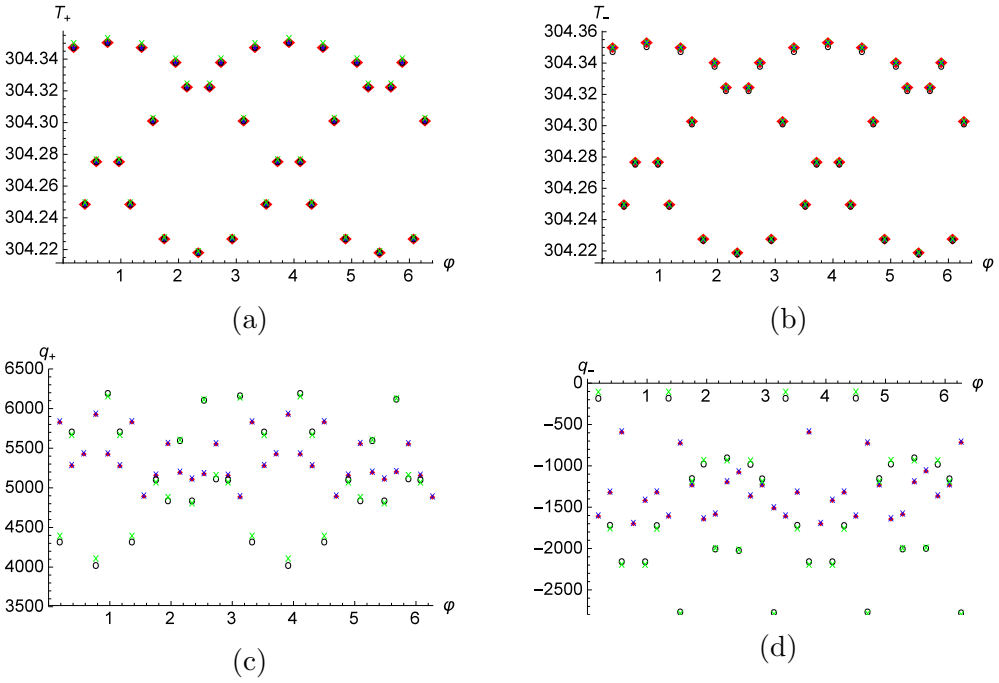

Figure 6: Temperatures (a) and (b) and heat fluxes (c) and (d) along the outer and inner boundaries for $n = 10$: the COMSOL solution (diamond-shaped and X-markers) and T and q evaluated through substitution of COMSOL data into the transmission conditions (x-markers and o-markers)

[3] Andreeva, D., Miszuris, W., Zagnetko, A., 2016. Transmission conditions for thin curvilinear close to circular heat-resistant interphases in composite ceramics. Journal of the European Ceramic Society 36 (9), 283–293.

[4] Benveniste, Y., 2006. A general interface model for a three-dimensional curved thin anisotropic interphase between two anisotropic media. Journal of the Mechanics and Physics of Solids 54, 708–734.

[5] Benveniste, Y., 2009. An interface model for a three-dimensional curved thin piezoelectric interphase between two piezoelectric media. Mathematics and Mechanics of Solids 14, 102–122.

[6] Borhan, A., Gromada, M., Samoila, P., Gherca, D., 2016. Fabrication and characterization of cubic $Ba_{0.5}Sr_{0.5}Co_{0.8}Fe_{0.2}O_{3-\beta}$ perovskite for a

novel "star-shaped" oxygen membrane with adeveloped surface. Materials Science and Engineering B 209, 66–74.

[7] Brun, M., Guenneau, S., Movchan, A., Bigoni, D., 2010. Dynamics of structural interfaces: Filtering and focussing effects for elastic waves. Journal of the Mechanics and Physics of Solids 58, 1212–1224.

[8] Brun, M., Movchan, A., Movchan, N., 2010. Shear polarisation of elastic waves by a structured interface. Continuum Mech. Thermodyn 22, 663–677.

[9] Burgess, J., Neugebauer, C., Flanagan, G., Moore, R., 1976. The direct bonding of metal to ceramics and application in electronics. Electrocomponent Science and Technology 2, 233–240.

[10] Castro, L., Kapanadze, D., Pesetskaya, E., December 2015. Effective conductivity of a compositematerial with stiff imperfect contact conditions. Methodical Methods in Applied Sciences 38 (18), 4638–4649.

[11] Cooper, G., 1971. The structure and mechanical properties of composite materials. Review of Physics in Technology 2, 49–91.

[12] Eremeyev, V., Rosi, G., Naili, S., 2016. Surface/interfacial anti-plane waves in solids with surface energy. Mechanics Research Communications 74, 8–13.

[13] Eremeyev, V. A., 2015. On effective properties of materials at the nano- and microscales considering surface effects. Acta Mechanica, 1–14.

[14] Every, A., Tzou, Y., Hasselman, D., Raj, R., January 1992. The effect of particle size on the thermal conductivity of zns/diamond composites. Acta Metallurgica et Materialia 40 (1), 123–129.

[15] Garrett, K., Rosenberg, H., 1974. The thermal conductivity of epoxy-resin/powder composite materials. Journal of Physics D: Applied Physics 7 (9), 1247–1258.

[16] Garrett, K., Rosenberg, H., 1975. The thermal conductivity of metal/dielectric-powder composites. Journal of Physics D: Applied Physics 8 (15), 1882–1888.

[17] Gei, M., 2008. Elastic waves guided by a material interface. European Journal of Mechanics A/Solids 27, 328–345.

[18] Jin, Z.-H., Batra, R., 1999. Thermal shock cracking in a metal-particle-reinforced ceramic matrix composite. Engineering Fracture Mechanics 62, 339–350.

[19] Lange, F., Velamakanni, B., Evans, A., 1990. Method for processing metal-reinforced ceramic composites. J. Am. Ceram. Soc. 73, 388–393.

[20] Lebon, F., Rizzoni, R., 2010. Asymptotic analysis of a thin interface: The case involving similar rigidity. International Journal of Engineering Science 48, 473–486.

[21] Lebon, F., Rizzoni, R., 2011. Asymptotic behavior of a hard thin linear elastic interphase: An energy approach. International Journal of Solids and Structures 48, 441–449.

[22] Mishuris, G., Miszuris, W., Öchsner, A., 2008. Evaluation of transmission conditions for thin reactive heat-conducting interphases. Defect Diffus. Forum 273-276, 394–399.

[23] Mishuris, G., Miszuris, W., Öchsner, A., 2009. Transmission conditions for thin reactive heat-conducting interphases: general case. Defect Diffus. Forum 283-286, 521–526.

[24] Mishuris, G., Öchsner, A., Kuhn, G., 2005. Fem-analysis of nonclassical transmission conditions between elastic structures part 1: Soft imperfect interface. Computers, Materials and Continua.

[25] Mishuris, G., Öchsner, A., Kuhn, G., 2006. Fem-analysis of nonclassical transmission conditions between elastic structures part 2: Stiff imperfect interface. Computers, Materials and Continua.

[26] Miszuris, W., Öchsner, A., 2013. Universal transmission conditions for thin reactive heat-conducting interphases. Continuum Mech. Thermodyn. 25, 1–21.

[27] Mityakov, A., et al., 2012. Gradient heat flux sensors for high temperature environments. Sensors and Actuators A 172, 1–9.

[28] Mogilevskaya, S., Crouch, S., 2004. A galerkin boundary integral method for multiple circular elastic inclusions with uniform interphase layers. International Journal of Solids and Structures 41, 1285–1311.

[29] Nairn, J., 2007. Numerical implementation of imperfect interfaces. Computational Materials Science 40, 525–536.

[30] Naumenko, K., Eremeyev, V. A., 2014. A layer-wise theory for laminated glass and photovoltaic panels. Composite Structures 112, 283–291.

[31] Naumenko, K., Eremeyev, V. A., 2017. A layer-wise theory of shallow shells with thin soft core for laminated glass and photovoltaic applications. Composite Structures 178, 434–446.

[32] Öchsner, A., Mishuris, G., 2008. A new finite element formulation for thin non-homogeneous heat-conducting adhesive layers. Journal of Adhesion Science and Technology 22, 1365–1378.

[33] Öchsner, A., Stasiek, M., Mishuris, G., Grácio, J., 2007. A new evaluation procedure for the butt-joint test of adhesive technology: Determination of the complete set of linear elastic constants. International Journal of Adhesion and Adhesives 27, 703–711.

[34] Pabst, R., Elssner, G., 1980. Adherence properties of metal-to-ceramic joints. Journal of Materials Science 15, 188–196.

[35] Qian, Z., Akisanya, A., Imbabi, M., 2000. Edge eects in the failure of elastic/viscoelastic joints subjected to surface tractions. International Journal of Solids and Structures 37, 5973–5994.

[36] Rizzoni, R., Lebon, F., 2012. Asymptotic analysis of an adhesive joint with mismatch strain. European Journal of Mechanics A/Solids 36, 1–8.

[37] Rizzoni, R., Lebon, F., 2013. Imperfect interphases as asymptotic models of thin curved elastic adhesive interphases. Mechanics Research Communications 51, 39–50.

[38] Sbaizero, O., Pezzotti, G., 2000. Tailoring the microstructure of a metal-reinforced ceramic matrix composite. Journal of Engineering Materials and Technology 122, 363–367.

[39] Steeves, C., He, M., Evans, A., 2009. The influence of coatings on the performance of structural heat pipes for hypersonic leading edges. Journal of the American Ceramic Society 92 (2), 553–555.

[40] Steeves, C., Mercer, C., Antinucci, E., He, M., Evans, A., 2009. Experimental investigation of the thermal properties of tailored expansion lattices. International Journal of Mechanics and Materials in Design 5 (2), 195–202.

[41] Ventola, L., Robotti, F., Dialameh, M., Calignano, F., Manfredi, D., Chiavazzo, E., Asinari, P., 2014. Rough surfaces with enhanced heat transfer for electronics cooling by direct metal laser sintering. International Journal of Heat and Mass Transfer 75, 58–74.

[42] Vitucci, G., Argatov, I., Mishuris, G., 2016. An asymptotic model for the deformation of a transversely isotropic, transversely homogeneous biphasic cartilage layer. Mathematical Methods in the Applied Sciences.